Flicker-Free Single Switch Multi-String LED Driver With High Power Factor and Current Balancing

Xueshan Liu, *Member, IEEE*, Xuewen Li, Qun Zhou, and Jianping Xu, *Member, IEEE*

***Abstract*—A flicker-free single switch multi-string LED driver with high power factor and current balancing is proposed and analyzed. It combines a pre-stage boost PFC converter and multiple second-stage buck dc–dc converters by a single active switch and multiple dc-link capacitors. With the proposed circuit configuration of multiple dc-link capacitors, the output current of each LED string can be balanced. Therefore, by controlling the output current of one LED string, the output currents of other LED strings can be controlled via current balancing of dc-link capacitors. The effect of the ripple of dc-link voltage on each output can be eliminated by fast voltage mode control loop. Therefore, flicker-free low ripple current for each LED string is achieved. With small voltage ripple across dc-link capacitors, the turn ON time of active switch is almost constant in a half line cycle. Therefore, power factor correction can be achieved with inductor current of pre-stage operating in discontinuous conduction mode (DCM). Finally, prototypes of dual-string LED driver with 90–135 Vac input and 175–265 Vac input for 47 W output power are built to verify the studied results.**

***Index Terms*—Current balancing, flicker-free, LED driver, multi-string, power factor correction (PFC), single switch.**

I. Introduction

HIGH brightness light emitting diode (HB-LED), with the distinct advantages of high light efficiency, fast response, environmental friendly, wide color gamut, long life span, and small size, is now renowned for extensive replacing conventional cold-cathode fluorescent lamps and incandescent lamps [1]–[4].

The brightness of LED is directly dependent on its forward current. For a single LED, the forward current and voltage are limited by its package. In order to achieve the required brightness and luminance uniformity, the simplest way is to connect several LEDs in series to form a LED string. However, for high-luminance applications, LED string with hundreds of LEDs connected in series leads to high output voltage of LED driver, which will cause reliability issue [5]. Therefore, several LED strings connected in parallel with acceptable terminal voltage

Manuscript received April 23, 2018; revised June 21, 2018 and August 30, 2018; accepted September 17, 2018. Date of publication September 30, 2018; date of current version May 2, 2019. This work was supported by the National Natural Science Foundation of China under Grant 51707126. Recommended for publication by Associate Editor F. J. Azcondo. *(Corresponding authors: Xueshan Liu and Qun Zhou.)*

X. Liu, X. Li, and Q. Zhou are with the College of Electrical Engineering and Information Technology, Sichuan University, Chengdu 610065, China (e-mail:

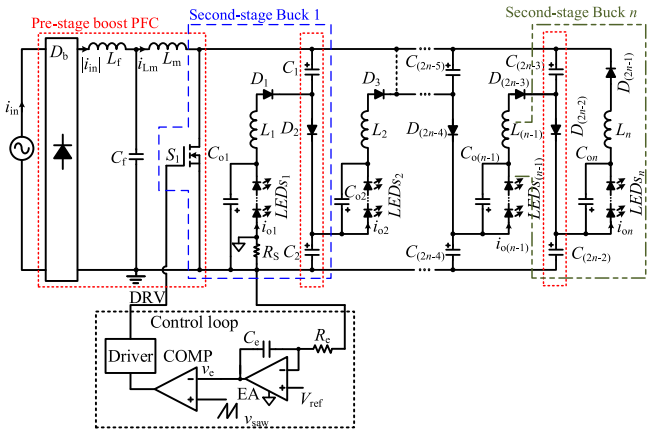

Fig. 1. Proposed n-string LED driver and its control loop.

In this paper, a flicker-free single switch multi-string LED driver with high power factor and passive current balancing is proposed and analyzed. It combines a pre-stage boost PFC converter and multiple second-stage buck dc–dc converters by a single active switch and multiple dc-link capacitors. Compared with conventional two-stage solution in [7], the proposed LED driver benefits with low cost of active power switch and control loop, while the dc-link capacitor is partitioned to each output branch for current balancing. Through reasonable design, the total volume and cost of dc-link capacitors can be closer to conventional solution in [7]. With the proposed circuit configuration of multiple dc-link capacitors, the current flowing through each LED string can be balanced. Therefore, by controlling the current of one LED string, the currents of other LED strings can be controlled via current balancing of dc-link capacitors.

In the proposed converter, the effect of dc-link voltage ripple on each output can be eliminated by fast voltage mode control loop. Therefore, flicker-free low ripple current of each LED string is achieved. With small voltage ripple on dc-link capacitors, the turn ON time of active switch is almost constant in a half line cycle. Therefore, power factor correction can be achieved with inductor current of pre-stage operating in discontinuous conduction mode (DCM). Finally, prototypes of dual-string LED driver with 90–135 Vac input and 175–265 Vac input for 47 W output power are built to verify the studied results.

II. Proposed Multi-String LED Driver

Fig. 1 shows the circuit of the proposed single switch n-string LED driver and its control loop. It combines a pre-stage boost PFC converter and multiple second-stage buck dc–dc converters by an active switch and multiple dc-link capacitors. The pre-stage boost PFC converter is composed of diode-bridge rectifier D_b, filter inductor L_f, filter capacitor C_f, magnetizing inductor L_m, active switch S_1, dc-link capacitors $C_{[k]}\,(k=1,2,\ldots,2n-2)$, and freewheel diodes $D_{[k]}\,(k=2,4,\ldots,2n-2)$. The buck 1 of second-stage is composed of a magnetizing inductor L_1, an active switch S_1, a output unit consisting of output capacitor C_{o1} and LED load LED_{s1}, dc-link capacitors C_1, C_2, and freewheel diodes D_1 and D_2. Similarly, the buck n of second-stage is composed of a magnetizing inductor L_n, an active switch S_1, a output unit consisting of output capacitor $C_{\rm on}$ and LED load LED_{sn}, dc-link capacitors $C_{(2n-2)}, C_{(2n-3)}$, and freewheel diodes $D_{(2n-1)}$ and $D_{(2n-2)}$. By voltage mode control loop, i_{o1} will be regulated to $V_{\rm ref}/R_s$, where R_s is the sample resistor of i_{o1}, and $V_{\rm ref}$ is the reference voltage of control loop. Meanwhile, $i_{o[k]}\,(k=2,3,\ldots,n)$ will be equal to i_{o1} via charge balancing of $C_{[k]}\,(k=1,2,\ldots,2n-2)$. Due to large capacitance of $C_{[k]}\,(k=1,2,\ldots,2n-2)$, voltage ripples across $C_{[k]}\,(k=1,2,\ldots,2n-2)$ can be effectively reduced. With fast voltage mode control loop, the effect of voltage ripples across $C_{[k]}\,(k=1,2,\ldots,2n-2)$ on each output current can be eliminated. Therefore, flicker-free low ripple LED current can be achieved. The turn ON time of switch S_1 can be considered constant in a half line cycle due to small voltage ripples across $C_{[k]}\,(k=1,2,\ldots,2n-2)$. Therefore, PFC can be realized with magnetizing inductor L_m operating in DCM.

In integrated PFC converter application, DCM operation modes of inductor currents of pre-stage and second-stage have advantage of high PF and simple control [35], [36]. In this paper, analysis and design considerations are presented when the currents flowing through $L_{[k]}\,(k=1,2,\ldots,n)$ and L_m operate in DCM. To simplify the analysis, other assumptions are made as follows.

1) All the components are assumed to be ideal.
2) The switching frequency f_s is much higher than the line frequency f_L.
3) The input voltage is a full-wave rectified sine wave, i.e., $|v_{\rm in}(t)| = V_p|\sin(\omega t)|$, where V_p is the amplitude and $\omega = 2\pi f_L$ is the angular frequency of ac input voltage.
4) The inductances of $L_{[k]}\,(k=1,2,\ldots,n)$ are equal, i.e., $L_1 = L_2 = \cdots = L_n$. The capacitances of dc-link capacitors $C_{[k]}\,(k=1,2,\ldots,2n-2)$ are equal, i.e., $C_1 = C_2 = \cdots = C_{(2n-2)}$.
5) Output capacitors $C_{o[k]}\,(k=1,2,\ldots,n)$ are large enough. Therefore, the voltages across them can be considered to be constant in a switching cycle. DC-link capacitors $C_{[k]}\,(k=1,2,\ldots,2n-2)$ are large enough. Therefore, the voltages across them can be considered to be constant in a half line cycle.

A. Current Balancing Among LED String

For the proposed n-string LED driver, as shown in Fig. 1, the averaged current of LED_{s1} is equal to the averaged current of diode D_2 in a switching cycle via the charge balance of dc-link capacitor C_1. Meanwhile, the averaged current of LED_{s2} is also equal to the averaged current of diode D_2 in a switching cycle via the charge balance of dc-link capacitor C_2. Therefore, the current balancing between LED_{s1} and LED_{s2} is achieved by dc-link capacitors C_1 and C_2. Similarly, the averaged current of $LED_{s(n-1)}$ is equal to the averaged current of diode $D_{(2n-2)}$ in a switching cycle via the charge balance of dc-link capacitor $C_{(2n-3)}$, and the averaged current of $LED_{s(n)}$ is equal to the averaged current of diode $D_{(2n-2)}$ in a switching cycle via the charge balance of dc-link capacitor $C_{(2n-2)}$. Therefore, the

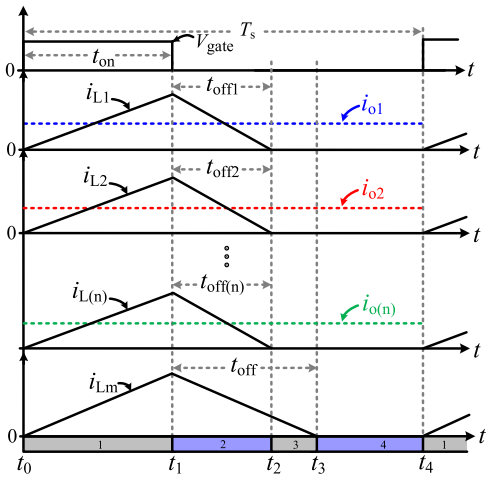

Fig. 2. Inductor current waveforms of the proposed LED driver in a switching cycle.

current balancing between $LED_{s(n-1)}$ and $LED_{s(n)}$ is achieved by dc-link capacitors $C_{(2n-3)}$ and $C_{(2n-2)}$. By the proposed circuit configuration of multiple dc-link capacitors, the average current of each LED string can be balanced.

In order to simplify the analysis, in this paper, the capacitances of dc-link capacitors $C_{[k]}$ $(k = 1, 2, \ldots, 2n-2)$ and inductances of $L_{[k]}$ $(k = 1, 2, \ldots, n)$ are assumed to be equal, respectively. In fact, according to the charge balance of dc-link capacitors, the output current balancing among LED strings is always satisfied even if $C_{[k]}$ $(k = 1, 2, \ldots, 2n-2)$ and $L_{[k]}$ $(k = 1, 2, \ldots, n)$ are not equal, respectively.

B. Inductor Currents of $L_{[k]}$ $(k = 1, 2, \ldots, n)$

As shown in Fig. 2, in a switching cycle, the average inductor currents $i_{L[k]\_av}$ $(k = 1, 2, \ldots, n)$ are equal to the output currents $i_{o[k]}$ $(k = 1, 2, \ldots, n)$, respectively, which can be expressed as

$$\begin{cases} i_{L1\_av} = i_{o1} = \dfrac{V_{C1} - V_{o1}}{2L_1 T_s} t_{\text{on}}(t_{\text{on}} + t_{\text{off}1}) \\ i_{L2\_av} = i_{o2} = \dfrac{V_{C2} + V_{C3} - V_{o2}}{2L_2 T_s} t_{\text{on}}(t_{\text{on}} + t_{\text{off}2}) \\ \quad \vdots \\ i_{L[n-1]\_av} = i_{o[n-1]} \\ = \dfrac{V_{C(2n-4)} + V_{C(2n-3)} - V_{o(n-1)}}{2L_{(n-1)} T_s} t_{\text{on}}(t_{\text{on}} + t_{\text{off}(n-1)}) \\ i_{L[n]\_av} = i_{o[n]} = \dfrac{V_{C(2n-2)} - V_{o(n)}}{2L_{(n)} T_s} t_{\text{on}}(t_{\text{on}} + t_{\text{off}(n)}) \end{cases} \tag{1}$$

where t_{on} is the turn ON time of switch S_1, $t_{\text{off}[k]}$ $(k = 1, 2, \ldots, n)$ are the time duration that $i_{L[k]}$ $(k = 1, 2, \ldots, n)$ freewheels through diodes $D_{(2[k]-3)}$ $(k = 1, 2, \ldots, n)$ when S_1 is turned OFF, $V_{C[k]}$ $(k = 1, 2, \ldots, 2n-2)$ are the voltages across capacitors $C_{[k]}$ $(k = 1, 2, \ldots, 2n-2)$, and $V_{o[k]}$ $(k = 1, 2, \ldots, n)$ are the voltages across $LED_{s[k]}$ $(k = 1, 2, \ldots, n)$, respectively.

The current balancing of each LED string is achieved by multiple dc-link capacitors, when the inductances of $L_{[k]}$ $(k = 1, 2, \ldots, n)$ are the same, there is

$$\begin{aligned} &(V_{C1} - V_{o1})(t_{\text{on}} + t_{\text{off}1}) = (V_{C2} + V_{C3} - V_{o2})(t_{\text{on}} + t_{\text{off}2}) \\ &\quad = \cdots = (V_{C(2n-4)} + V_{C(2n-3)} - V_{o(n-1)})(t_{\text{on}} + t_{\text{off}(n-1)}) \\ &\quad = (V_{C(2n-2)} - V_{o(n)})(t_{\text{on}} + t_{\text{off}(n)}). \end{aligned} \tag{2}$$

In a switching cycle, by applying the voltage-second balance of inductors $L_{[k]}$ $(k = 1, 2, \ldots, n)$, it gives rise to

$$\begin{cases} (V_{C1} - V_{o1})t_{\text{on}} = (V_{C2} + V_{o1})t_{\text{off}1} \\ (V_{C2} + V_{C3} - V_{o2})t_{\text{on}} = (V_{C4} + V_{o2} - V_{C2})t_{\text{off}2} \\ \quad \vdots \\ (V_{C(2n-4)} + V_{C(2n-3)} - V_{o(n-1)})t_{\text{on}} = (V_{C(2n-2)} \\ + V_{o(n-1)} - V_{C(2n-4)})t_{\text{off}(n-1)} \\ (V_{C(2n-2)} - V_{o(n)})t_{\text{on}} = (V_{C(2n-3)} + V_{o(n)})t_{\text{off}(n)}. \end{cases} \tag{3}$$

From Fig. 1, in a switching cycle, the following equation can be obtained:

$$\begin{aligned} V_{C1} + V_{C2} &= V_{C3} + V_{C4} = \cdots = V_{C(2n-5)} + V_{C(2n-4)} \\ &= V_{C(2n-3)} + V_{C(2n-2)}. \end{aligned} \tag{4}$$

From (2)–(4), there is

$$t_{\text{off}1} = t_{\text{off}2} = \cdots = t_{\text{off}(n-1)} = t_{\text{off}(n)}. \tag{5}$$

Substituting (5) into (1) and (3), the following equation can be obtained:

$$\begin{aligned} &V_{C1} - V_{o1} = V_{C2} + V_{C3} - V_{o2} = \cdots = V_{C(2n-4)} + V_{C(2n-3)} \\ &\quad - V_{o(n-1)} = V_{C(2n-2)} - V_{o(n)} \end{aligned} \tag{6}$$

$$\begin{aligned} &V_{C2} + V_{o1} = V_{C4} + V_{o2} - V_{C2} = \cdots = V_{C(2n-2)} + V_{o(n-1)} \\ &\quad - V_{C(2n-4)} = V_{C(2n-3)} + V_{o(n)}. \end{aligned} \tag{7}$$

According to (6) and (7), the voltages across $L_{[k]}$ $(k = 1, 2, \ldots, n)$ during the time duration of t_{on} and $t_{\text{off}[k]}$ $(k = 1, 2, \ldots, n)$ are the same, respectively. Based on (5), the time duration of freewheeling inductor current of $L_{[k]}$ $(k = 1, 2, \ldots, n)$ are all equal. Therefore, when the inductances of $L_{[k]}$ $(k = 1, 2, \ldots, n)$ are the same, the inductor currents $i_{L[k]}$ $(k = 1, 2, \ldots, n)$ are all equal, i.e., $i_{L1} = i_{L2} = \cdots = i_{L(n)}$.

C. Capacitor Voltages of $C_{[k]}$ $(k = 1, 2, \ldots, 2n-2)$

In a switching cycle, the rectified input current $|i_{\text{in}}(t)|$ is equal to the average current of L_m, which can be given as

$$|i_{\text{in}}(t)| = i_{Lm\_av}(t) = \frac{V_p |\sin \omega t| t_{\text{on}}(t_{\text{on}} + t_{\text{off}})}{2L_m T_s} \tag{8}$$

where t_{off} is the duration of freewheeling time of inductor current i_{Lm} when S_1 is turned OFF.

Based on voltage-second balance of magnetizing inductor L_m, there is

$$V_p |\sin \omega t| t_{\text{on}} = (V_{C1} + V_{C2} - V_p |\sin \omega t|) t_{\text{off}}. \tag{9}$$

In a half line cycle, the average input power is equal to the output power, there is

$$P_{\text{in}} = \frac{2}{T_L}\int_0^{T_L/2} v_{\text{in}}(t) i_{\text{in}}(t)dt = \frac{V_p(V_{C1}+V_{C2})t_{\text{on}}^2}{2\pi L_m T_s} \times \int_0^{\pi} \frac{\sin^2\omega t}{(V_{C1}+V_{C2})/V_p - |\sin\omega t|}d\omega t = P_o. \quad (10)$$

When $1.1 < (V_{C1}+V_{C2})/V_{\text{p}} < 5$, by using curve fitting method, the following equation is almost equal:

$$\frac{1}{\pi}\int_0^{\pi} \frac{\sin^2\omega t}{(V_{C1}+V_{C2})/V_p - |\sin\omega t|}d\omega t \approx \frac{0.48}{(V_{C1}+V_{C2})/V_p - 0.95}. \quad (11)$$

According to (8)–(11), the voltages across dc-link capacitors can be expressed as

$$V_{C1}+V_{C2} = V_{C3}+V_{C4} = \cdots = V_{C(2n-3)}+V_{C(2n-2)} = \frac{1.9V_pL_mT_sP_o}{2L_mT_sP_o - 0.48V_p^2t_{\text{on}}^2}. \quad (12)$$

From (6), (7), and (12), the voltages across dc-link capacitors can be, respectively, calculated. In this paper, a proposed dual-string LED driver will be analyzed, as an example in Section III, including its detail analysis and design considerations.

III. Analysis and Design Considerations of Proposed Dual-String LED Driver

A. Operating Modes

When the currents flowing through inductors L_1, L_2, and L_m operate in DCM, the steady-state waveforms of the proposed dual-string LED driver includes four operating modes in a switching cycle. The theoretical waveforms and corresponding equivalent circuits are shown in Figs. 3 and 4, respectively. There are two different operation conditions between t_2 and t_3 : $t_{Lm-\text{dis}} > t_{L1-\text{dis}}$ (or $t_{L2-\text{dis}}$) and $t_{Lm-\text{dis}} < t_{L1-\text{dis}}$ (or $t_{L2-\text{dis}}$), which are shown in Fig. 3(a) and (b), respectively, where $t_{Lm-\text{dis}}$ is the duration of freewheeling time of inductor current i_{Lm} when S_1 is turned OFF, and $t_{L1-\text{dis}}$ (or $t_{L2-\text{dis}}$) is the duration of freewheeling time of inductor current i_{L1} (or i_{L2}) when S_1 is turned OFF.

Mode 1 [t_0, t_1]: At time t_0, switch S_1 is turned ON. The power is delivered from voltage source $|v_{\text{in}}|$ to magnetizing inductor L_m, the magnetizing inductor current i_{Lm} increases linearly

$$i_{Lm}(t) = \frac{|v_{\text{in}}|}{L_m}(t-t_0). \quad (13)$$

Meanwhile, diode D_2 is turned OFF under reverse bias voltage $(V_{c1}+V_{c2})$. The power is delivered from dc-link capacitors C_1 and C_2 to inductors L_1 and L_2 through diodes D_1 and D_3, respectively. The inductor currents i_{L1} and i_{L2} and the capacitor currents i_{C1} and i_{C2} can be expressed as

$$\begin{cases} i_{L1}(t) = \frac{V_{C1}-V_{o1}}{L_1}(t-t_0) \\ i_{L2}(t) = \frac{V_{C2}-V_{o2}}{L_2}(t-t_0) \\ i_{C1}(t) = -i_{L1}(t) \\ i_{C2}(t) = -i_{L2}(t). \end{cases} \quad (14)$$

When switch S_1 is turned OFF, this mode is ended. The time duration of this mode is $\tau_1 = t_1 - t_0 = t_{\text{on}}$.

Mode 2 [t_1, t_2]: At time t_1, switch S_1 is turned OFF. Diode D_2 is conducted to provide a current flowing path for $i_{Lm}(t)$. Similarly, D_1 and D_3 are still conducted to provide the current flowing paths for $i_{L1}(t)$ and $i_{L2}(t)$. In this mode, inductor currents i_{Lm}, i_{L1} and i_{L2} decrease linearly. The state equations in this mode can be obtained as

$$\begin{cases} i_{Lm}(t) = i_{Lm}(t_1) + \frac{|v_{\text{in}}|-V_{C1}-V_{C2}}{L_m}(t-t_1) \\ i_{L1}(t) = i_{L1}(t_1) + \frac{-V_{C2}-V_{o1}}{L_1}(t-t_1) \\ i_{L2}(t) = i_{L2}(t_1) + \frac{-V_{C1}-V_{o2}}{L_2}(t-t_1) \end{cases} \quad (15)$$

$$\begin{cases} i_{C1}(t) = i_{Lm}(t) + i_{L2}(t) \\ i_{C2}(t) = i_{Lm}(t) + i_{L1}(t). \end{cases} \quad (16)$$

Input voltage $|v_{\text{in}}(t)|$ is sinusoidal in a half line cycle, which causes a sinusoidal variation of $t_{Lm-\text{dis}}$. Therefore, there are two different operation conditions when this mode is ended: $t_{Lm-\text{dis}} > t_{L1-\text{dis}}$ (or $t_{L2-\text{dis}}$) and $t_{Lm-\text{dis}} < t_{L1-\text{dis}}$

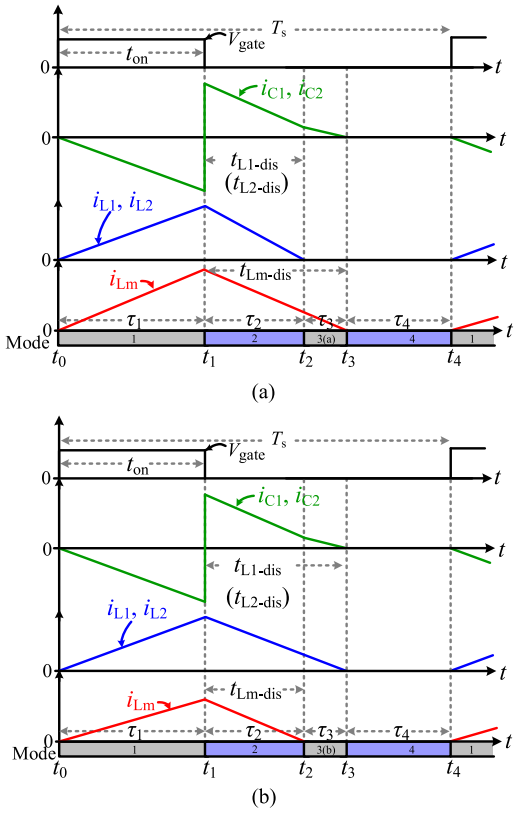

Fig. 3. Steady-state waveforms of the proposed LED driver. (a) $t_{Lm-\text{dis}} > t_{L1-\text{dis}}$ (or $t_{L2-\text{dis}}$). (b) $t_{Lm-\text{dis}} < t_{L1-\text{dis}}$ (or $t_{L2-\text{dis}}$).

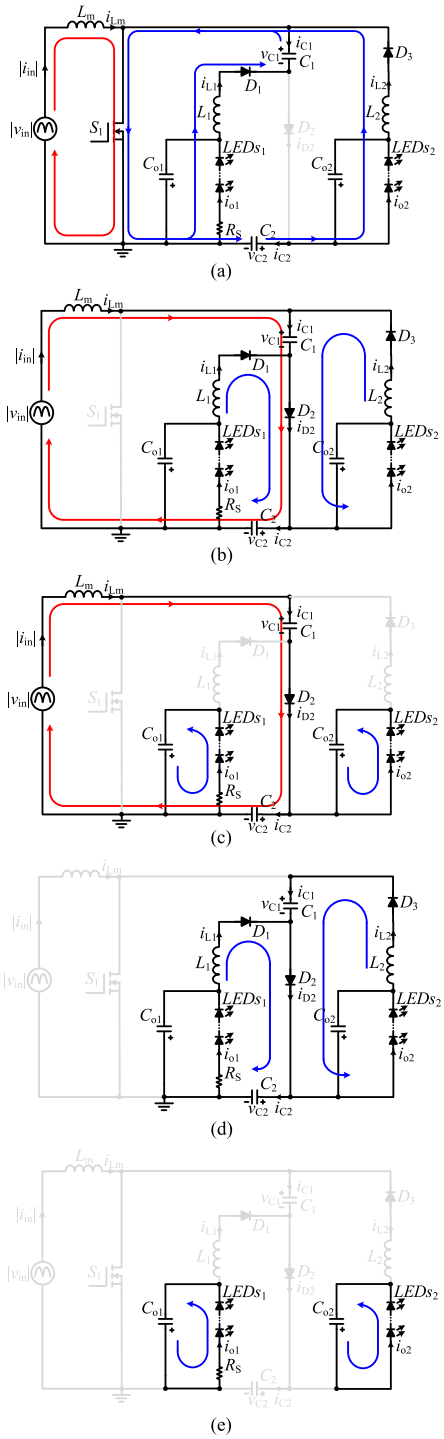

Fig. 4. Equivalent circuits of the proposed dual-string LED driver. (a) Mode 1 $[t_0, t_1]$. (b) Mode 2 $[t_1, t_2]$. (c) Mode 3-a $[t_2, t_3]$. (d) Mode 3-b $[t_2, t_3]$. (e) Mode 4 $[t_3, t_4]$.

(or $t_{L2-\mathrm{dis}}$). When $t_{Lm-\mathrm{dis}} > t_{L1-\mathrm{dis}}$ (or $t_{L2-\mathrm{dis}}$), at time t_2, i_{L1} and i_{L2} decrease to zero simultaneously. Diodes D_1 and D_3 are turned OFF at zero current and Mode 2 is ended. The circuit will enter into next operation mode, Mode 3-a. In this case, the time duration of Mode 2 is

$$\tau_2 = t_2 - t_1 = \frac{i_{L1}(t_1)L_1}{V_{C2} + V_{o1}} = \frac{i_{L2}(t_1)L_2}{V_{C1} + V_{o2}}. \tag{17}$$

When $t_{Lm-\mathrm{dis}} < t_{L1-\mathrm{dis}}$ (or $t_{L2-\mathrm{dis}}$), at time t_2, i_{Lm} first decrease to zero. Mode 2 is ended at time t_2 and the circuit will enter into next operation mode, Mode 3-b. In this case, the time duration of Mode 2 is

$$\tau_2 = t_2 - t_1 = \frac{i_{Lm}(t_1)L_m}{V_{C1} + V_{C2} - |v_{\mathrm{in}}|}. \tag{18}$$

Mode 3-a $[t_2, t_3]$: At time t_2, switch S_1 is still turned OFF and diode D_2 is still turned ON. Diodes D_1 and D_3 are reverse-biased due to the inductor currents i_{L1} and i_{L2} are decreased to zero. The magnetizing inductor current i_{Lm} still decreases linearly. At time $t_3, i_{Lm}(t)$ decreases to zero. Diodes D_2 is turned OFF at zero current and this mode is ended. The state equations in this mode can be obtained as

$$\begin{cases} i_{Lm}(t) = i_{Lm}(t_2) + \frac{|v_{\mathrm{in}}| - V_{C1} - V_{C2}}{L_m}(t - t_2) \\ i_{L1}(t) = i_{L2}(t) = 0 \\ i_{C1}(t) = i_{C2}(t) = i_{Lm}(t). \end{cases} \tag{19}$$

The time duration of Mode 3-a is

$$\tau_3 = t_3 - t_2 = \frac{i_{Lm}(t_2)L_m}{V_{C1} + V_{C2} - |v_{\mathrm{in}}|}. \tag{20}$$

Mode 3-b $[t_2, t_3]$: At time t_2, switch S_1 is still turned OFF and diode D_1, D_2, and D_3 are still turned ON. The magnetizing inductor current i_{Lm} is decreased to zero. Both inductor currents i_{L1} and i_{L2} still decrease linearly. At time t_3, i_{L1} and i_{L2} decrease to zero simultaneously. Diodes D_1, D_2, and D_3 are turned OFF at zero current and this mode is ended. The state equations in this mode can be obtained as

$$\tau_3 = t_3 - t_2 = \frac{i_{L1}(t_2)L_1}{V_{C2} + V_{o1}} = \frac{i_{L2}(t_2)L_2}{V_{C1} + V_{o2}}. \tag{21}$$

Mode 4 $[t_3, t_4]$: As shown in Fig. 4(e), switch S_1, diodes D_1, D_2, and D_3 are all turned OFF. i_{Lm}, i_{L1}, and i_{L2} are all zero. Output currents of two LED strings are provided by output capacitors C_{o1} and C_{o2}. This operation mode will be ended and a switching cycle is over at time t_4. The time duration of this mode is $\tau_4 = t_4 - t_3 = T_s - \tau_3 - \tau_2 - \tau_1$.

B. Input Current

Fig. 5 shows the key waveforms of the proposed dual-string LED driver in a line cycle. The peak current of magnetizing inductor L_m can be expressed as

$$i_{Lm\_pk} = \frac{|v_{\mathrm{in}}(t)|t_{\mathrm{on}}}{L_m} = \frac{V_p|\sin\omega t|dT_s}{L_m} \tag{22}$$

where d is the turn ON duty cycle of S_1.

Based on voltage-second balance of magnetizing inductor L_m, there is

$$V_p|\sin\omega t|dT_s = (V_{C1} + V_{C2} - V_p|\sin\omega t|)d_1T_s \tag{23}$$

where d_1 is the duty ratio of freewheeling time of inductor current i_{Lm} when S_1 is turned OFF.

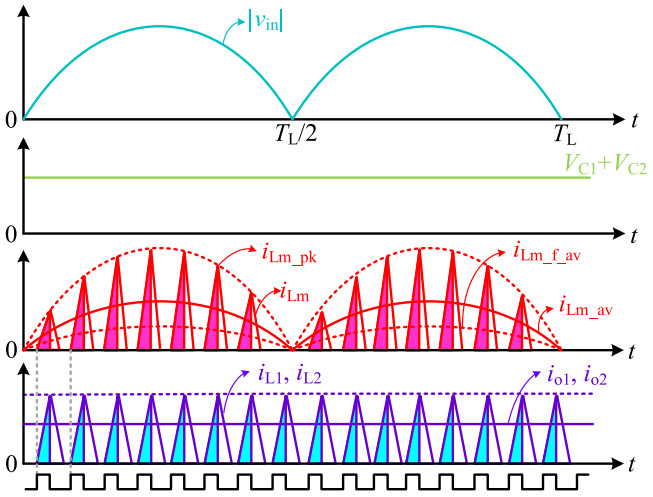

Fig. 5. Key waveforms of the proposed LED driver in a line cycle.

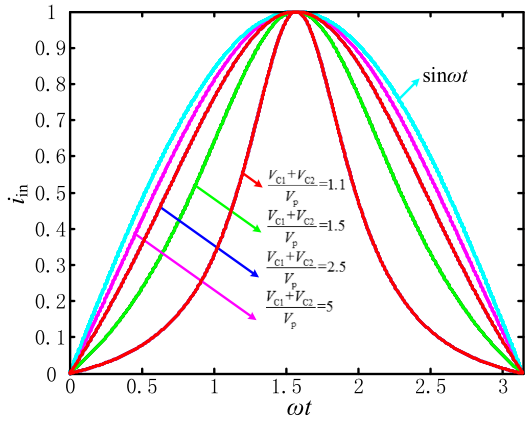

Fig. 6. Normalized input current waveform with different $(V_{C1}+V_{C2})/V_p$.

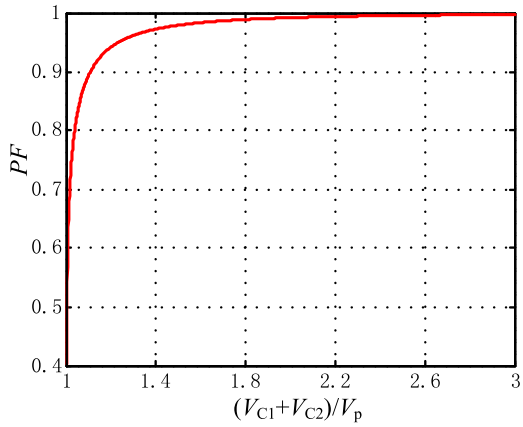

Fig. 7. Relationship of *PF* and $(V_{C1}+V_{C2})/V_p$.

According to (3) and (23), there are

$$M_1=\frac{V_{C1}+V_{C2}}{v_{\rm in}}=\frac{d+d_1}{d_1} \tag{24}$$

$$M_2=\frac{V_{o1}+V_{o2}}{V_{C1}+V_{C2}}=\frac{d-d_2}{d+d_2} \tag{25}$$

$$M=\frac{V_{o1}+V_{o2}}{v_{\rm in}}=\frac{(d+d_1)(d-d_2)}{d_1(d+d_2)} \tag{26}$$

where M_1 is the voltage gain of boost stage, M_2 is the voltage gain of buck stages, M is the voltage gain of the proposed LED driver, and d_2 is the duty ratio of freewheeling time of inductor current i_{L1} (or i_{L2}) when S_1 is turned OFF.

From (24)–(26), a step-down voltage gain can be achieved by regulating the turn ON duty ratio of switch S_1.

In a switching cycle, the rectified input current $|i_{\rm in}(t)|$ is equal to the average current of L_m, which can be given as

$$|i_{\rm in}(t)|=i_{Lm\_av}(t)=\frac{V_p|\sin\omega t|d(d+d_1)T_s}{2L_m}. \tag{27}$$

From (26) and (27), the rectified current $|i_{\rm in}(t)|$ can further be written as

$$|i_{\rm in}(t)|=i_{Lm\_av}(t)=\frac{V_p d^2T_s(V_{C1}+V_{C2})|\sin\omega t|}{2L_m(V_{C1}+V_{C2}-V_p|\sin\omega t|)}. \tag{28}$$

Fig. 6 is plotted according to (28). It can be known that the distortion of input current waveforms is related to $(V_{C1}+V_{C2})/V_p$. With larger $(V_{C1}+V_{C2})/V_p$, the distortion of input current will be smaller.

The average input power in a half line cycle is

$$\begin{aligned}P_{\rm in}&=\frac{2}{T_L}\int_0^{T_L/2}v_{\rm in}(t)i_{\rm in}(t)dt\\&=\frac{V_p(V_{C1}+V_{C2})d^2T_s}{2\pi L_m}\int_0^{\pi}\frac{\sin^2\omega t}{(V_{C1}+V_{C2})/V_p-|\sin\omega t|}d\omega t.\end{aligned} \tag{29}$$

According to (28) and (29), *PF* of the proposed dual-string LED driver operating in DCM can be derived as

$$\begin{aligned}PF&=\frac{P_{\rm in}}{\frac{V_p}{\sqrt{2}}\sqrt{\frac{2}{T_L}\int_0^{T_L/2}(i_{\rm in}(t))^2dt}}\\&=\frac{\frac{\sqrt{2}}{\pi}\int_0^{\pi}\frac{\sin^2\omega t}{1-V_p\sin\omega t/(V_{C1}+V_{C2})}d\omega t}{\sqrt{\frac{1}{\pi}\int_0^{\pi}\frac{\sin^2\omega t}{[1-V_p\sin\omega t/(V_{C1}+V_{C2})]^2}d\omega t}}.\end{aligned} \tag{30}$$

Fig. 7 is plotted according to (30), from which it can be known that *PF* increases with the increase of $(V_{C1}+V_{C2})/V_p$.

C. Design Considerations of DC-Link Voltage

Assume that dc-link capacitors, C_1 and C_2 are large enough. In a half line cycle, the output power can described as

$$\begin{aligned}\frac{2}{T_L}\int_0^{T_L/2}v_{\rm in}(t)i_{\rm in}(t)dt&=(V_{o1}+V_{o2})i_{o1}\\&=(V_{o1}+V_{o2})(i_{L1\_m\_av}+i_{L2\_m\_av}-i_{Lm\_f\_av})\end{aligned} \tag{31}$$

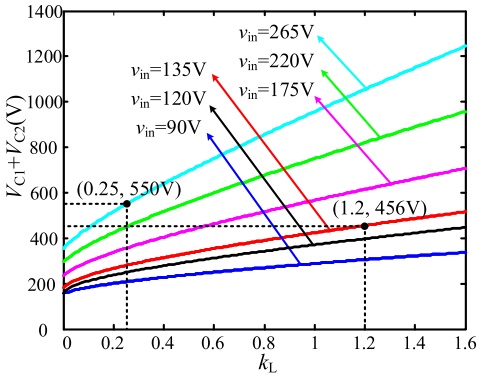

Fig. 8. Relationship of $V_{C1}+V_{C2}$ and k_L ($V_{o1}=V_{o2}=78$ V).

where

$$\begin{cases} i_{L1\_m\_av} = \frac{(V_{C1}-V_{o1})t_{\rm on}^2}{2L_1T_s} \\ i_{L2\_m\_av} = \frac{(V_{C2}-V_{o2})t_{\rm on}^2}{2L_2T_s} \\ i_{Lm\_f\_av} = \frac{2}{T_L}\int_0^{T_L/2}\frac{|v_{\rm in}|t_{\rm on}t_{\rm off}}{2L_mT_s}dt. \end{cases} \tag{32}$$

According to (29), (31), and (32), the relationship between output voltage and dc-link capacitor voltage can be given as

$$V_{C1}+V_{C2} = \frac{(0.95\ V_p+V_o)}{2} + \frac{0.24k_LV_p^2}{V_o} + \sqrt{\left(\frac{(0.95\ V_p+V_o)}{2}+\frac{0.24k_LV_p^2}{V_o}\right)^2 - (0.95\ V_pV_o - 0.48k_LV_p^2)} \tag{33}$$

where $V_o=V_{o1}+V_{o2}$, $k_L=L_1/L_m$.

From (6), (7), and (33), the voltages across C_1 and C_2 can be, respectively, expressed as

$$V_{C1} = 0.5(V_{C1}+V_{C2})+0.5(V_{o1}-V_{o2}) \tag{34}$$

$$V_{C2} = 0.5(V_{C1}+V_{C2})+0.5(V_{o2}-V_{o1}). \tag{35}$$

From (33), the relationship of $V_{C1}+V_{C2}$ and k_L can be illustrated in Fig. 8, with the output voltage $V_{o1}=V_{o2}=78$ V. From Fig. 8, it can be known that the sum of capacitor voltages $V_{C1}+V_{C2}$ increases with k_L. As shown in Figs. 7 and 8, k_L should be designed as high as possible to achieve high *PF*. However, the reverse voltage v_{S1} of S_1 is equal to the sum of capacitor voltages $V_{C1}+V_{C2}$. In order to reduce the voltage stress of switch S_1, the ratio k_L must be controlled in a reasonable range. From Fig. 8, it can be known that through reasonable design of k_L, the voltage stress of dc-link capacitors can be designed lower. Therefore, the total volume and cost of dc-link capacitors can be decreased, which can be closer to conventional solution in [7]. In order to achieve good performance of efficiency and PF with consideration of voltage stress, the proposed LED driver is more suitable for narrow input voltage range application. Considering above design guideline, k_L is designed to be 1.2 for 90–135 Vac input and 0.25 for 175–265 Vac input in this paper.

D. Design Considerations of L_1, L_2, and L_m

Assume that dc-link capacitors C_1 and C_2 are large enough. From (22), when $|\sin\omega t|=1$, the maximum peak current of magnetizing inductor L_m can be expressed as

$$i_{Lm\_pk\_\max} = \frac{V_pdT_s}{L_m}. \tag{36}$$

When the inductor current of L_m operates in a critical conduction mode (CRM) at maximum input voltage in a half line cycle, there is

$$i_{Lm\_pk\_\max} = 2i_{Lm\_av\_\max} \tag{37}$$

where $i_{Lm\_av\_\max}$ is the maximum average current of L_m in a half line cycle.

According to (28), (36), and (37), when L_m operates in a CRM at maximum input voltage in a half line cycle, the critical turn ON duty cycle of switch S_1 can be derived as

$$d_{Lm}^c = \frac{V_{C1}+V_{C2}-V_p}{V_{C1}+V_{C2}}. \tag{38}$$

Substituting (38) into (31), the critical inductance of L_m can be derived as

$$L_m^c = \frac{0.48V_p^2(V_{C1}+V_{C2}-V_p)^2}{2P_of_s(V_{C1}+V_{C2})(V_{C1}+V_{C2}-0.95V_p)}. \tag{39}$$

Similarly, when inductor current of L_1 operates in CRM, the critical condition can be given as

$$i_{L1\_pk} = 2i_{L1\_av} \tag{40}$$

where

$$i_{L1\_pk} = \frac{(V_{C1}-V_{o1})dT_s}{L_1} \tag{41}$$

$$i_{L1\_av} = i_{o1} = \frac{(V_{C1}-V_{o1})(t_{\rm on}+t_{\rm off1})t_{\rm on}}{2L_1T_s}. \tag{42}$$

From (40), when inductor current of L_1 operates in CRM, the critical turn ON duty cycle of switch S_1 can be given as

$$d_{L1}^c = \frac{V_{C1}+V_{o1}}{V_{C1}+V_{C2}}. \tag{43}$$

Substituting (43) into (31), the critical inductance of L_1 and L_2 can be derived as

$$L_1^c = L_2^c = \frac{(V_{C1}-V_{o1})(V_{C2}+V_{o1})}{2i_of_s(V_{C1}+V_{C2})}. \tag{44}$$

According to (39), (44), and the analysis results of Section III-C, Fig. 9 shows the relationship between L_1^c, L_2^c, L_m^c and input voltage $v_{\rm in}$ with $v_{o1}=v_{o2}=78$ V, $i_{o1}=i_{o2}=0.3$ A and $f_s=67$ kHz. As shown in Fig. 9, the critical inductances of L_1, L_2, and L_m all increase with the increase of input voltage $v_{\rm in}$. The minimum critical inductances are obtained at $v_{\rm in}=90$ Vac for 90–135 Vac input and $v_{\rm in}=175$ Vac for 175–265 Vac input, respectively. Therefore, L_m should be designed less than 0.69 mH for 90–135 Vac input and 1.28 mH for 175–265 Vac input, respectively. Considering design margin and current stress, in this paper, L_m and L_1 (L_2) are set to 0.56 mH and 0.68 mH for 90–135 Vac input, and are set to 1.1 mH and 0.275 mH for 175–265 Vac input, respectively.

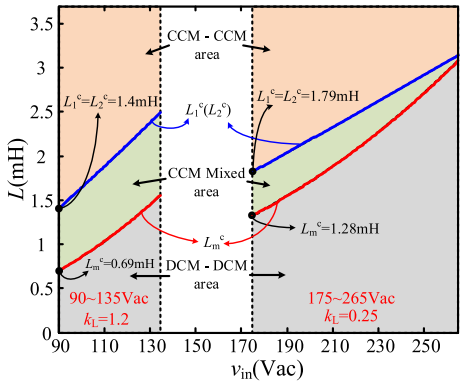

Fig. 9. Operation area of the proposed LED driver.

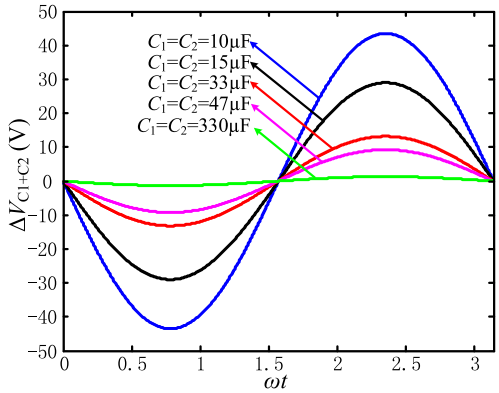

Fig. 10. Variation of voltage ripples of dc-link capacitor with different C_1 and C_2.

E. Design Considerations of C_1 and C_2

The analysis in Section III-C and D are based on the assumption that the dc-link capacitors C_1 and C_2 are large enough. The ideal parameter for dc-link capacitor is difficult to realize due to the limit of circuit volume in practical application. Therefore, the effects of voltage ripple across C_1 and C_2 need to be considered due to small capacitances are selected. Due to the unbalance of instantaneous power between pulsating input power and fixed output power, the dc-link capacitor is needed to equilibrate the instantaneous power, which results in line frequency voltage ripple across dc-link capacitors. In general, it only needs to consider the second harmonic component of voltage ripple that can meet the requirement of analysis.

The average current flowing through diode D_2 in a switching cycle can be derived as

$$i_{Lm\_f\_av}(t) = \frac{V_p|\sin\omega t|t_{\rm on}t_{\rm off}}{2L_mT_s} = \frac{V_p^2t_{\rm on}^2\sin^2\omega t}{2L_mT_s(V_{C1}+V_{C2}-V_p|\sin\omega t|)}. \quad (45)$$

With Fourier decomposition, (45) can be further described as

$$i_{Lm\_f\_av}(t) = \frac{a_0}{2} + \sum_{n=1}^{\infty} a_n\cos n\omega t \quad (46)$$

where

$$a_0 = \frac{2}{\pi}\int_0^{\pi} i_{Lm\_f\_av}(t)d\omega t \quad (47)$$

$$a_n = \frac{2}{\pi}\int_0^{\pi} i_{Lm\_f\_av}(t)\cos n\omega t d(\omega t) = \begin{cases} 0 & n \text{ is odd} \\ \dfrac{2V_p^2t_{\rm on}^2}{\pi L_mT_s}\displaystyle\int_0^{\frac{\pi}{2}}\frac{\sin^2\omega t\cos n\omega t}{V_{C1}+V_{C2}-V_p\sin\omega t}d(\omega t) & n \text{ is even.} \end{cases} \quad (48)$$

The second-order harmonic component of $i_{Lm\_f\_av}$ flowing though dc-link capacitors leads to the second-order line frequency voltage ripple. Therefore

$$\Delta v_{C1+C2}(t) = \frac{C_1+C_2}{C_1C_2}\int i_{Lm\_f\_av[2]}(t)dt \quad (49)$$

where

$$i_{Lm\_f\_av[2]}(t) = a_2\cos(2\omega t). \quad (50)$$

According to (48) and (49), the voltage ripple can be calculated as

$$\Delta v_{C1+C2}(t) = \frac{C_1+C_2}{C_1C_2}\frac{V_p^2t_{\rm on}^2\sin(2\omega t)}{\omega\pi L_mT_s}\int_0^{\frac{\pi}{2}}\frac{\sin^2\omega t\cos 2\omega t}{V_{C1}+V_{C2}-V_p\sin\omega t}d(\omega t). \quad (51)$$

In this paper, the capacitances of dc-link capacitors are set to the same. Therefore, the voltage ripples across C_1 and C_2 can be given as

$$\Delta v_{C1}(t) = \Delta v_{C2}(t) = \frac{\Delta v_{C1+C2}(t)}{2}. \quad (52)$$

Based on the analysis results of Section III-C and III-D, Fig. 10 shows the variations of voltage ripple across dc-link capacitor with different C_1 and C_2 in a line cycle, from which it can be known that with the larger capacitance of C_1 and C_2, the variation of voltage ripple ΔV_{C1+C2} will be smaller.

According to (28) and (51), the rectified input current $|i_{\rm in}|$ with second-order harmonic component can be described as

$$|i_{\rm in}(t)| = \frac{V_pd^2T_s(V_{C1}+V_{C2}+\Delta V_{C1+C2})|\sin\omega t|}{2L_m(V_{C1}+V_{C2}+\Delta V_{C1+C2}-V_p|\sin\omega t|)}. \quad (53)$$

From (53), the normalized input current waveforms with different C_1 and C_2 are shown in Fig. 11. There is a discernible distortion in the waveforms of input current, as shown in Fig. 11. With smaller capacitance of C_1 and C_2, the distortion of input current waveform will be more serious. Specially, when C_1 and C_2 are greater than 47 μF, the distortion of input current waveform is not obvious, which can be used as the design guideline of C_1 and C_2, i.e., $C_1 = C_2 = 47$ μF.

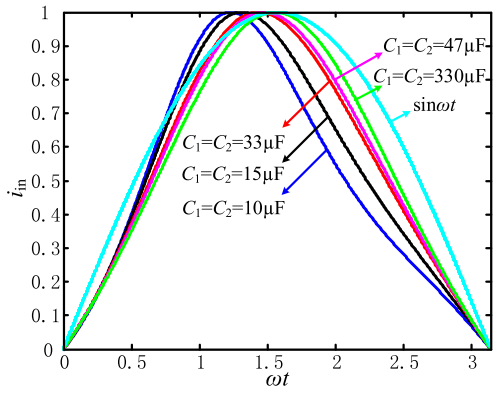

Fig. 11. Normalized input current waveform with different C_1 and C_2.

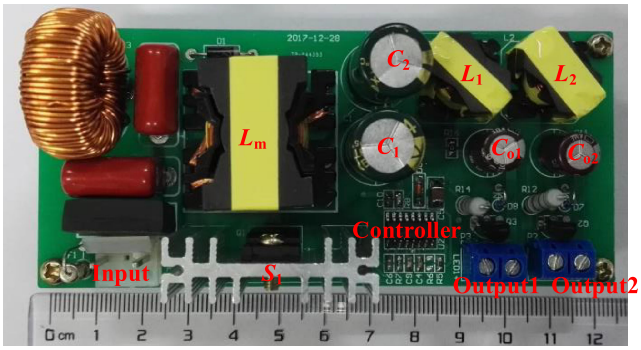

Fig. 12. Photo of 90–135 Vac input prototype.

IV. Experimental Verification

To verify above analysis, prototypes of the proposed dual-string LED driver with 90–135 Vac input and 175–265 Vac input for 47 W output power are built. Fig. 12 shows the photo of 90–135 Vac input prototype. The schematic and corresponding parameters of the prototypes are shown in Fig. 4 and Table I, respectively.

According to the analysis in Section III, with $k_L = 1.2$, the voltage stress of S_1 can be controlled below 456 V for 90–135 Vac input. With $k_L = 0.25$, the voltage stress of S_1 can be controlled below 550 V for 175–265 Vac input. Therefore, MOSFET 15NM65 with 650 V drain-source voltage is used in both 90–135 Vac input and 175–256 Vac input prototypes. A conventional voltage mode controller, Texas Instruments TL494, is used in these prototypes.

The input current waveforms of the proposed LED driver at rated output power are shown in Fig. 13. From which it can be known that input current i_{in} is sinusoidal and in phase with input voltage v_{in}. *PF* of these two prototypes are shown in Fig. 14. It can be known that *PF* of these two prototypes are higher than 0.97 within wide input voltage range. Therefore, the proposed LED driver has a good performance of *PF*.

Harmonic current under 120 and 220 Vac input are shown in Fig. 15. According to Fig. 15, each harmonic component (up to 15th) of input current is lower than the limit of IEC-61000-3-2 Class C with large margins. The total harmonic distortion of input current is 9.61% and 20.92% in 120 Vac and 220 Vac input, respectively.

TABLE I
Circuit Parameters of Two 47 W Prototype

Variable	Definition	Value
v_{o1}~ v_{o2}	Rated voltage of each LED output	78 V LED string
i_{o1}	Output Current of LED_{s1}	0.3 A
S_1	Power MOSFET	15NM65
D_1~D_4	Freewheeling diode	KBL608
C_1~ C_2	Dc link capacitor	47 μF/400 V
C_{o1}~C_{o2}	Output capacitor	22 μF/100 V
L_f	Input filter inductance	470 μH
f_s	Switching Frequency	67 kHz
	FOR 90~135Vac Input	
L_m	Magnetizing inductance	560 μH
L_1~ L_2	Inductance of buck stage	680 μH
C_f	Input filter capacitance	680 nF
	FOR 175~265Vac Input	
L_m	Magnetizing inductance	1100 μH
L_1~ L_2	Inductance of buck stage	275 μH
C_f	Input filter capacitance	220 nF

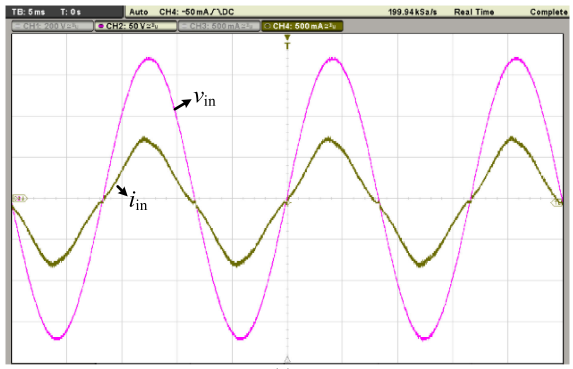

(a)

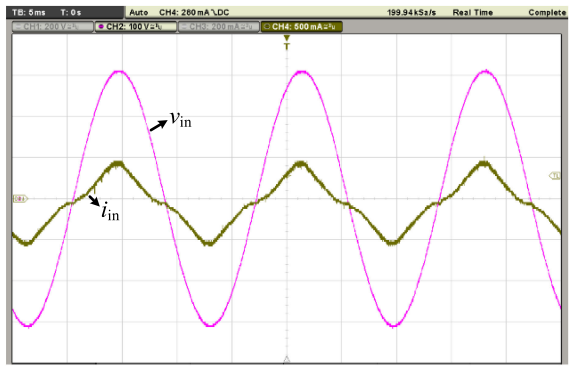

(b)

Fig. 13. v_{in} and i_{in} waveforms of the proposed dual-string LED driver. (a) 120 Vac (90–135 Vac input prototype). (b) 220 Vac (175–265 Vac input prototype).

Fig. 16 shows the voltage waveform of switch S_1, inductor current waveforms under 120 Vac input and 220 Vac input. According to the Fig. 16, it can be known that i_{Lm}, i_{L1}, and i_{L2} all operate in DCM. The current waveforms of i_{L1} and

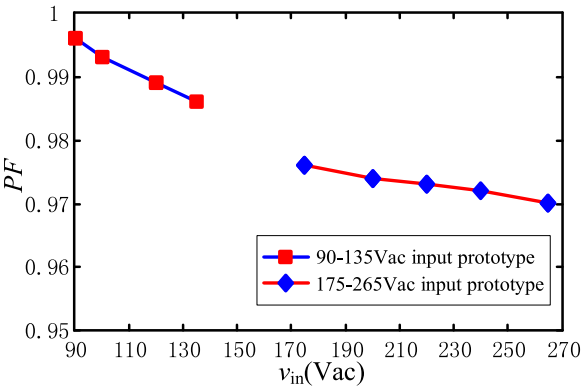

Fig. 14. *PF* of the proposed dual-string LED driver.

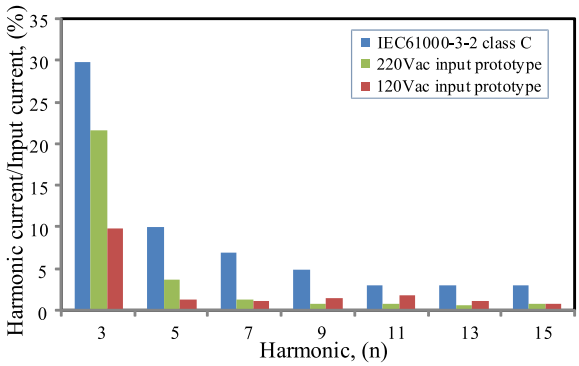

Fig. 15. Harmonic test results of input current i_{in}.

TABLE II
OUTPUT CURRENT UNDER RATED LOAD

Output	v_{in} (Vac)					
	90~135Vac input prototype			175~265Vac input prototype		
	90	120	135	175	220	265
i_{o1} (mA)	300.9	301.5	301.6	299.7	300.0	300.2
v_{o1} (V)	80.19	80.31	80.26	79.84	79.67	79.69
i_{o2} (mA)	300.7	301.2	301.3	299.5	299.8	300.1
v_{o2} (V)	79.92	80.03	79.99	77.38	77.25	77.26

i_{L2} are almost the same, which verifies the analysis results in Section II-B.

The output voltages and currents under rated LED load and extreme LED load imbalance are given in Tables II and III. From Tables II and III, it can be known that the output currents of two LED strings are almost the same under different output loads, which shows good performance of current balancing among two LED strings.

The startup waveforms of 90–135 Vac input prototype are shown in Fig. 17. It can be known that balanced output currents are quickly established after startup. The ripple on LED current may be a potentially health hazard to human eyes, which has been recommended in IEEE Standard 1789-2015 [37]. From

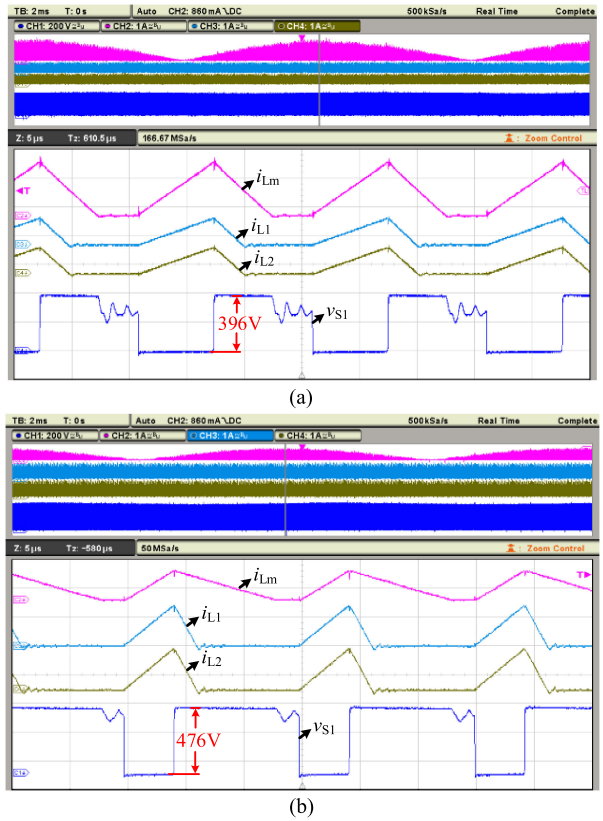

Fig. 16. i_{Lm}, i_{L1}, i_{L2}, and v_{S1} of the proposed LED driver. (a) 120 Vac input. (b) 220 Vac input.

TABLE III
OUTPUT CURRENT UNDER EXTREME LOAD IMBALANCE

Output	v_{in} (Vac)					
	90~135Vac input prototype			175~265Vac input prototype		
	90	120	135	175	220	265
i_{o1} (mA)	301.1	301.4	301.8	299.6	300.1	300.3
v_{o1} (V)	80.13	80.30	80.22	79.69	79.79	79.77
i_{o2} (mA)	300.9	301.2	301.7	299.3	299.9	300.2
v_{o2} (V)	44.55	44.66	44.61	42.53	42.59	42.58

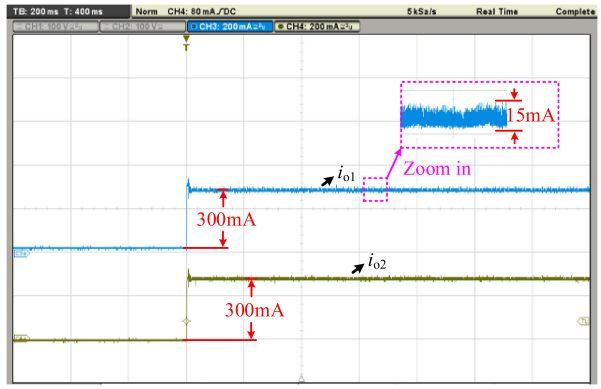

Fig. 17. Startup waveforms of the proposed LED driver in 120 Vac input.

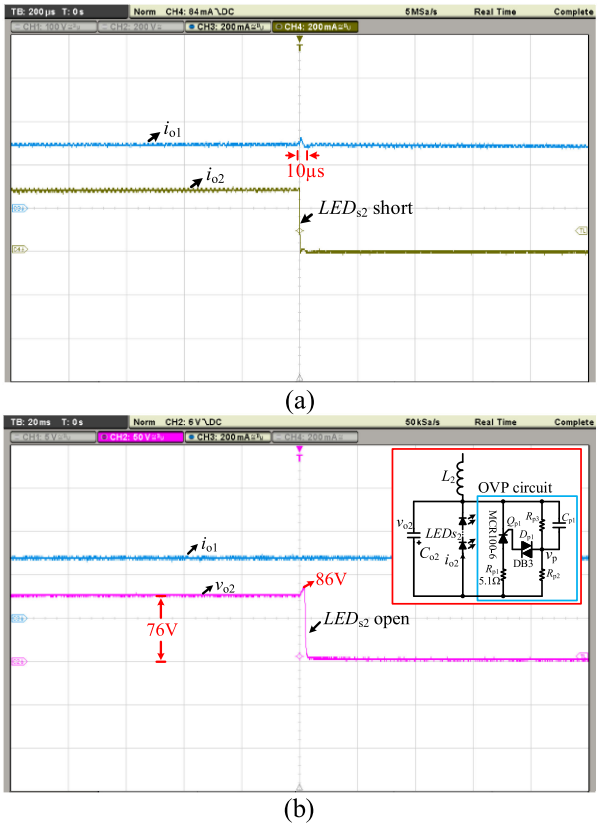

Fig. 18. Dynamic balancing response waveforms (90–135 Vac input). (a) LED_{s2} is short-circuit. (b) LED_{s2} is open-circuit.

[37], it can be known that the percentage of flicker, Mod%, can be expressed as follows:

$$\text{Mod}\% = \frac{\text{Max} - \text{Min}}{\text{Max} + \text{Min}} \times 100\% \tag{54}$$

where Max and Min represent maximum and minimum light intensity from the lamp, respectively. When $f_L = 60$ Hz, the low-risk level leads to Mod% $< 10\%$. Assume that the light intensity is proportional to the LED current. In Fig. 17, the output current ripple is below 15 mA, Mod% $= 2.5\%$. Therefore, flicker-free low-risk LED current is achieved.

Fig. 18 shows the dynamic balancing response waveforms. As shown in Fig. 18(a), when LED_{s2} is short-circuit, the output current of LED_{s1} still keeps balance after a small transient overshoot. For LED driver application with constant current control, the output voltage will increase continuously if LED string is open-circuit. The continuously increased voltage will damage the LED driver. Therefore, over-voltage-protection (OVP) circuit is needed. In the prototype, OVP circuits are placed in each output. When LED_{s2} is open-circuit, the waveforms and corresponding circuit schematic of OVP are shown in Fig. 18(b). The OVP circuit consists of a SCR switch Q_{p1} (MCR100-6), a trigger diode D_{p1} (DB3), a current limit resistor R_{p1} (5.1 Ω), and voltage divider consisting of R_{p2}, R_{p3}, and C_{p1}. When the divided voltage v_p is increased to the trigger voltage of D_{p1}, SCR switch Q_{p1} will be triggered. Output 2 will be shorted by

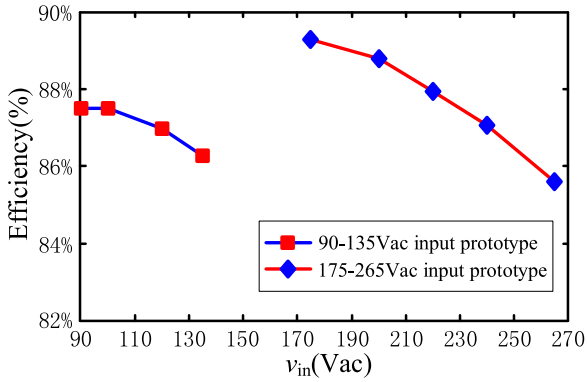

Fig. 19. Efficiency curve of the proposed dual-string LED driver.

Q_{p1} and R_{p1}. Therefore, v_{o2} will be clamped to a low voltage level and the output 1 can still operate normally. From the experiment waveforms, it can be known that the OVP trigger voltage is about 86 V. Similarly, when output 1 is opened, the output voltage v_{o1} will be clamped to a low level. But the average current flowing through R_s is still controlled to the required level. Therefore, i_{o2} is not changed when LED_{s1} is opened. Fig. 18 shows a good dynamic balancing characteristic of the proposed LED driver.

Fig. 19 shows the efficiency of the proposed dual-string LED driver. As shown in Fig. 19, the maximum efficiency of 90–135 Vac prototype and 175–265 Vac prototype are 87.8% and 89.7%, respectively. Therefore, the proposed dual-string LED driver has good efficiency performance.

V. Conclusion

A flicker-free single switch multi-string LED driver with high power factor and passive current balancing is proposed and analyzed. It combines a pre-stage boost PFC converter with second-stage buck dc–dc converters by a single active switch and dc-link capacitors. With the proposed dc-link capacitors connection method, the output current of each LED string is balanced. Therefore, by controlling the output current of one LED string, the output currents of other LED strings can be controlled, which simplifies circuit design. The effect of dc-link voltage ripple on each output is eliminated by fast voltage mode control loop of second-stage circuit. Therefore, flicker-free low ripple current of each LED string is achieved. With small voltage ripple on dc-link capacitors, the turn ON time of active switch is almost constant in a half line cycle. Therefore, power factor correction is achieved. Experimental results are presented to verify the analysis results of the proposed driver, and demonstrate its advantages. The proposed scheme needs only one active switch and one control loop, which makes circuit volume small and cost low. In fact, the proposed scheme comes from an integration of a two-stage solution. The inductor currents of two stages flow though the shared switch. The current and voltage stress should be considered carefully in design. This solution can be easily applied to high power multi-string LED lighting such as panel lighting application.

REFERENCES

[1] X. Qu, S.-C. Wong, and C. K. Tse, "Resonance-assisted buck converter for offline driving of power LED replacement lamps," *IEEE Trans. Power Electron.*, vol. 26, no. 2, pp. 532–540, Feb. 2011.

[2] S.-C. Moon, G.-B. Koo, and G.-W. Moon, "Dimming-feedback control method for TRIAC dimmable LED drivers" *IEEE Trans. Ind. Electron.*, vol. 62, no. 2, pp. 960–965, Feb. 2015.

[3] E. S. Lee, B. H. Choi, D. T. Nguyen, G. C. Jang, and C. T. Rim, "Versatile LED drivers for various electronic ballasts by variable switched capacitor," *IEEE Trans. Power Electron.*, vol. 31, no. 2, pp. 1489–1502, Feb. 2016.

[4] N. Chen and H. S.-H. Chung, "A driving technology for retrofit LED lamp for fluorescent lighting fixtures with electronic ballasts," *IEEE Trans. Power Electron.*, vol. 26, no. 2, pp. 588–601, Feb. 2011.

[5] C. Zhao, X. Xie, and S. Liu, "Multioutput LED drivers with precise passive current balancing," *IEEE Trans. Power Electron.*, vol. 28, no. 3, pp. 1438–1448, Mar. 2013.

[6] X. Qu, S.-C. Wong, and C. K. Tse, "A current balancing scheme with high luminous efficacy for high-power LED lighting," *IEEE Trans. Power Electron.*, vol. 29, no. 6, pp. 2649–2654, Jun. 2014.

[7] M. Arias, D. G. Lamar, F. F. Linera, D. Balocco, A. A. Diallo, and J. Sebastián, "Design of a soft-switching asymmetrical half-bridge converter as second stage of an LED driver for street lighting application," *IEEE Trans. Power Electron.*, vol. 27, no. 3, pp. 1608–1621, Mar. 2012.

[8] Q. Xiaohui, S.-C. Wong, and C.-K. Tse, "Noncascading structure for electronic ballast design for multiple LED lamps with independent brightness control," *IEEE Trans. Power Electron.*, vol. 25, no. 2, pp. 331–340, Feb. 2010.

[9] U. Hu and M. M. Jovanovic, "LED *driver* with self-adaptive drive voltage," *IEEE Trans. Power Electron.*, vol. 23, no. 6, pp. 3116–3125, Nov. 2008.

[10] S. N. Li and S. Y. R. Hui, "Self-configurable current-mirror circuit with short-circuit and open-circuit fault tolerance for balancing parallel light-emitting diode (LED) string currents," *IEEE Trans. Power Electron.*, vol. 29, no. 10, pp. 5498–5507, Oct. 2014.

[11] H. Chen, Y. Zhang, and D. Ma, "A SIMO parallel-string driver IC for dimmable LED backlighting with local bus voltage optimization and single time-shared regulation loop," *IEEE Trans. Power Electron.*, vol. 27, no. 1, pp. 452–462, Jan. 2012.

[12] W.-H. Yang, H.-A. Yang, C.-J. Huang, and K. H. Chen, "A high-efficiency single-inductor multiple-output buck-type LED driver with average current correction technique," *IEEE Trans. Power Electron.*, vol. 33, no. 4, pp. 3375–3385, Apr. 2018.

[13] Q. Luo, S. Zhi, C. Zou, W. Lu, and L. Zhou, "A LED driver with dynamic high frequency sinusoidal bus voltage regulation for multi-string applications," *IEEE Trans. Power Electron.*, vol. 29, no. 1, pp. 491–500, Jan. 2014.

[14] R. Zhang and H. S.-H. Chung, "Capacitor-isolated multistring LED driver with daisy-chained transformers," *IEEE Trans. Power Electron.*, vol. 30, no. 7, pp. 3860–3875, Jul. 2015.

[15] X. Qu, S.-C. Wong, and C. K. Tse, "An improved LCLC current-source-output multistring LED driver with capacitive current balancing," *IEEE Trans. Power Electron.*, vol. 30, no. 10, pp. 5783–5791, Oct. 2015.

[16] S. Choi and T. Kim, "Symmetric current-balancing circuit for LED backlight with dimming," *IEEE Trans. Ind. Electron.*, vol. 59, no. 4, pp. 1698–1707, Apr. 2012.

[17] J. Zhang, J. Wang, and X. Wu, "A capacitor-isolated LED driver with inherent current balance capability," *IEEE Trans. Ind. Electron.*, vol. 59, no. 4, pp. 1708–1716, Apr. 2012.

[18] X. Wu, J. Zhang, and Z. Qian, "A simple two-channel LED driver with automatic precise current balancing," *IEEE Trans. Ind. Electron.*, vol. 58, no. 10, pp. 4783–4788, Oct. 2011.

[19] X. Wu, J. Zhang, and Z. Qian, "Analysis and design considerations of LLCC resonant multioutput DC DC LED driver with charge balancing and exchanging of secondary series resonant capacitors," *IEEE Trans. Power Electron.*, vol. 30, no. 2, pp. 780–789, Feb. 2015.

[20] *Electromagnetic Compatibility (EMC), Part 3-2: Limits–limits for harmonic current emissions (equipment current ≤ 16 A per phase), International Standard* IEC 61000-3-2, 2009.

[21] C. K. Tse, M. H. L. Chow, and M. K. H. Cheung, "A family of PFC voltage regulator configurations with reduced redundant power processing," *IEEE Trans. Power Electron.*, vol. 16, no. 6, pp. 794–802, Nov. 2001.

[22] X. Liu, J. Xu, Z. Chen, and N. Wang, "Single-inductor dual-output buck-boost power factor correction converter," *IEEE Trans. Ind. Electron.*, vol. 62, no. 2, pp. 943–952, Feb. 2015.

[23] X. Liu, Q. Yang, Q. Zhou, J. Xu, and G. Zhou, "Single-stage single-switch four-string resonant LED driver with high power factor and passive current balancing," *IEEE Trans. Power Electron.*, vol. 32, no. 6, pp. 4566–4576, Jun. 2017.

[24] P. Fang, Y.-J. Qiu, H. Wang, and Y.-F. Liu, "A single-stage primary-side-controlled off-line flyback LED driver with ripple cancellation," *IEEE Trans. Power Electron*, vol. 32, no. 6, pp. 4700–4715, Jun. 2017.

[25] B. Lehman and A. J. Wilkins, "Designing to mitigate the effects of flicker in LED lighting," *IEEE Power Electron., Mag.*, vol. 1, no. 3, pp. 18–26, Sep. 2014.

[26] A. Wilkins, J. Veitch, and B. Lehman, "LED lighting flicker and potential health concern: IEEE standard PAR1798 update," in *Proc. IEEE Conf.*, 2010, pp. 171–178.

[27] G. M. Soares, P. S. Almeida, J. M. Alonso, and H. A. C. Braga, "Capacitance minimization in offline LED drivers using an active-ripple-compensation technique," *IEEE Trans. Power Electron.*, vol. 32, no. 4, pp. 3022–3033, Apr. 2017.

[28] S. Wang, X. Ruan, K. Yao, S.-C. Tan, Y. Yang, and Z. Ye, "A flicker-free electrolytic capacitor-less AC–DC LED driver," *IEEE Trans. Power Electron.*, vol. 27, no. 11, pp. 4540–4548, Nov. 2012.

[29] J. He, X. Ruan, and L. Zhang, "Adaptive voltage control for bidirectional converter in flicker-free electrolytic capacitor-less AC–DC LED driver," *IEEE Trans. Ind. Electron.*, vol. 64, no. 1, pp. 320–324, Jan. 2016.

[30] P. Fang, Y.-F. Liu, and P. C. Sen, "A flicker-free single-stage offline LED driver with high power factor," *IEEE J. Emerg. Sel. Topics Power Electron.*, vol. 3, no. 3, pp. 654–665, Sep. 2015.

[31] H.-C. Kim, M. C. Choi, S. Kim, and D.-K. Jeong, "An AC–DC LED driver with a two-parallel inverted buck topology for reducing the light flicker in lighting applications to low-risk levels," *IEEE Trans. Power Electron.*, vol. 32, no. 5, pp. 3879–3891, May 2017.

[32] Y. Qiu, L. Wang, H. Wang, Y.-F. Liu, and Paresh C. Sen, "Bipolar ripple cancellation method to achieve single-stage electrolytic-capacitor-less high-power LED driver," *IEEE J. Emerg. Sel. Topics Power Electron.*, vol. 3, no. 3, pp. 698–713, Sep. 2015.

[33] P. Fang and Y.-F. Liu, "Energy channeling LED driver technology to achieve flicker-free operation with true single stage power factor correction," *IEEE Trans. Power Electron.*, vol. 32, no. 5, pp. 3892–3907, May 2017.

[34] H. Valipour, G. Rezazadeh, and M. R. Zolghadri, "Flicker-free electrolytic capacitor-less universal input offline LED driver with PFC," *IEEE Trans. Power Electron.*, vol. 31, no. 9, pp. 6553–6561, Sep. 2016.

[35] O. L. Santos, L. Martinez-Salamero, and G. Garcia, "Steady-state analysis of inductor conduction modes in the quadratic boost converter," *IEEE Trans. Power Electron.*, vol. 31, no. 2, pp. 1489–1502, Feb. 2016.

[36] T. Yan, J. Xu, Z. Dong, L. Shu, and P. Yang, "Quadratic boost PFC converter with fast dynamic response and low output voltage ripple," in *Proc. IEEE Int. Conf. Commun. Circuits Syst.*, 2013, pp. 402–406.

[37] *IEEE Recommended Practices for Modulating Current in High-Brightness LEDs for Mitigating Health Risks to Viewers*, IEEE Standard 1789-2015, Jun. 2015.

Xueshan Liu (M'18) received the B.S. degree in communication engineering and the M.S. and Ph.D. degrees in electrical engineering from Southwest Jiaotong University, Chengdu, China, in 2005, 2010, and 2016, respectively.

From 2005 to 2008, he worked as Development Engineer for switching mode power supplies in Asia Power Devices. Inc., Shenzhen, China. He is currently a Lecturer with the College of Electrical Engineering and Information Technology, Sichuan University. His research interests include control technique of switching mode power supply, power factor correction converters, and the application of power electronic systems.

Xuewen Li received the B.S. degree in electrical engineering and automation from the School of Electrical Engineering, Zhengzhou University, Zhengzhou, China, in 2016. He is currently working toward the M.S. degree in the College of Electrical Engineering and Information Technology at Sichuan University, Chengdu, China.

His research interests include power factor correction converter and development of new converter topologies.

Qun Zhou received the M.S. and Ph.D. degrees in automation engineering from the University of Electronic Science and Technology of China, Chengdu, China, in 1989 and 2009, respectively.

She is currently a Professor with the College of Electrical Engineering and Information Technology, Sichuan University. Her research interests include power quality analysis and control.

Jianping Xu (M'10) received the B.S. and Ph.D. degrees in electronic engineering from the University of Electronics Science and Technology of China, Chengdu, Sichuan, China, in 1984 and 1989, respectively.

Since 1989, he has been with the School of Electrical Engineering, Southwest Jiaotong University, Chengdu, China, where he has been a Professor since 1995. From November 1991 to February 1993, he was with the Department of Electrical Engineering, University of Federal Defense Munich, Munich, Germany, as a Visiting Research Fellow. From February 1993 to July 1994, he was with the Department of Electrical Engineering and Computer Science, University of Illinois at Chicago, Chicago, IL, USA, as a Visiting Scholar. His research interests include modeling, analysis, and control of power electronic systems.